Multiple-scattering theoretical approach to scanning tunneling microscopy

Kamal K. Saha,* Jürgen Henk, Arthur Ernst, and Patrick Bruno
Max-Planck-Institut für Mikrostrukturphysik, Weinberg 2, D-06120 Halle (Saale), Germany
(Received 25 June 2007; revised manuscript received 14 October 2007; published 25 February 2008)

An approach for computing scanning tunneling microscopy from first principles is proposed. Within the framework of Landauer-Büttiker theory, the conductance of a scanning tunneling microscope (STM) is obtained in terms of real-space Green functions, thereby taking into account incoherent tunneling processes and the tip-sample interaction but avoiding repeated STM tips as in a supercell approach. The approach is formulated within multiple-scattering theory, especially in the Korringa-Kohn-Rostoker method, but can be implemented in any Green-function method for electronic-structure calculations. Extensive tests are presented for planar and STM tunnel junctions involving Au(111) electrodes.

DOI: 10.1103/PhysRevB.77.085427 PACS number(s): 68.37.Ef, 72.10.−d, 73.40.Gk

I. INTRODUCTION

The invention of the scanning tunneling microscope (STM) by Binnig and Rohrer (see Ref. 1 for a review) was a revolution in surface physics. The ability to probe locally surfaces and adsorbates on the atomic scale led to new experimental methods and new insights that were impossible to obtain by other advanced methods (such as photoelectron spectroscopy or low-energy-electron diffraction).[2] In order to interpret STM experiments qualitatively and quantitatively, there have been numerous efforts to formulate a theory of the STM,[3] preferably within the framework of first-principles electronic-structure calculations.

The probably most widely used model was proposed by Tersoff and Hamann[4,5] (TH) who, applying the transfer-Hamiltonian approach of Bardeen,[6] express the tunnel current by the density of states of the sample at the position of the STM tip. By this means, the tunnel current becomes independent of the electronic properties of the tip. This feature obviously contradicts experiments that find indeed a dependence of the tunnel current on the tip and its preparation conditions. Astonishingly, the TH model works well provided the surface density of states is computed by advanced first-principles methods, such as the full-potential linearized augmented plane wave or the full-potential Korringa-Kohn-Rostoker (KKR) method.[7] For example, the corrugation and the magnetic contrast in spin-resolved STM (see, e.g., Ref. 8) agree qualitatively and semiquantitatively with experimental results (without any claim of completeness, we refer to Refs. 9–14).

However, the TH model approximates crudely the tunnel matrix elements that can essentially determine the tunnel current. A step beyond the TH model is the transfer-Hamiltonian approach in which the matrix elements are computed from the wave functions of the sample and the tip.[15,16] In order to distinguish unequivocally the tip wave function from the sample wave function, the entire tunnel junction is divided into two subsystems, namely, the sample and tip, and the electronic structures of these subsystems are calculated separately. Therefore, tip-sample interactions, which might be significant for small tip-sample distances, are not included.[17]

Both of the above-mentioned theories rely solely on the electronic structures of sample and tip but neglect the boundary conditions, in particular reservoirs attached to the leads. Tunneling is a scattering process and, hence, scattering boundary conditions have to be applied, as is done in the Landauer-Büttiker theory of electronic transport. Within this respect, the conductance of a tunnel junction can be viewed as transmission.[18] One particular way to obtain the transmission probability can be regarded as the "electron-counting" picture: the conductance is proportional to the rate at which electrons are transmitted from one lead to the other. To obtain this rate, the electrons in the reservoirs are counted before and after establishing a connection of the otherwise disconnected leads. This approach can be formulated via the Green functions of the decoupled and coupled subsystems (see Sec. II C).

The above Landauer-Büttiker approach has a number of advantages as compared to other approaches. (i) It considers the role of reservoirs and obeys scattering boundary conditions. (ii) The electronic structures of both leads and tunnel barrier are fully taken into account. Since an *ab initio* calculation is performed for the entire tunnel junction, the effect of tip-sample interactions is fully accounted for, in contrast to the Bardeen approach. (iii) By solving the Dyson equation for the STM tip in real space (configuration space), a system with a single tip is treated. This feature is different from supercell approaches in which an artificial periodicity might lead to spurious errors due to "cross talk" between adjacent STM tips.[19,20] (iv) It can be implemented in a variety of methods for electronic-structure calculations which rely on Green functions, in particular tight-binding and multiple-scattering methods. We note in passing that Green functions provide a means to incorporate substitutional disorder via the coherent potential approximation.[21–23]

In order to implement the outlined approach for a STM, a computational scheme is needed that can deal with large systems.[24] Besides tight-binding methods, multiple-scattering theory is an obvious choice. [We would like to mention explicitly the tight-binding or screened versions of the KKR method[25–28] and of the linear muffin-tin orbital method.[29]] The latter has proven its suitability for treating a variety of problems with high accuracy; to name a few, bulk and surface electronic properties, electron spectroscopies such as low-energy-electron diffraction and photoelectron spectroscopy, substitutional disorder in alloys, etc.[30] The accuracy, as high as for other advanced methods, is evident, for

example, from computations of the magnetic anisotropy of ultrathin films[31,32] and of the dispersion of surface states.[33,34] With this background in mind, a multiple-scattering theory of scanning tunneling microscopy was implemented in a spin-polarized relativistic layer KKR computer code, which is described and applied in the present paper. Although the number of advantages is significant (see previous paragraph), no approach is, of course, without shortcomings. These are discussed in Sec. II D. We would like to emphasize that the approach is not restricted to tunneling through a vacuum barrier; transport in nanocontacts (e.g., atomic point contacts or nanowires) can be treated as well.

The paper is organized as follows. The basic theory is outlined in Sec. II, sketching a KKR formulation of the conductance calculations in real space. The scheme is applied to scanning tunneling spectroscopy on Au(111),[35,36] addressing in particular the effect of a STM tip on the conductance. The paper concludes with remarks given in Sec. IV.

II. THEORY

A. Introductory remarks

Since the following sections are rather technical, it appears helpful to start with a brief outline of the approach. A scanning tunneling microscope can be viewed as built from three subsystems: the ideal leads of the sample and of the tip side, respectively, and the tunnel barrier, which comprises the STM tip and the lead surfaces. These subsystems are joined at so-called decoupling—or coupling—regions L and R (L and R stand for the left and right decoupling regions, respectively). Since Landauer-Büttiker theory will be applied, for each of the steps discussed below two Green function (GFs) have to be computed: one for the system with decoupled subsystems, the other for the system with coupled subsystems (cf. the electron-counting picture mentioned in Sec. I).[37] The conductance of the STM is computed in real space from the final GFs.

The computational procedure is as follows. (i) Green functions are computed in reciprocal space for tunnel junctions with decoupled and coupled subsystems. These systems do not include the STM tip and, thus, are translationally invariant parallel to the layers. Hence, the in-plane wave vector $\boldsymbol{k}_\parallel$ is a good quantum number. (ii) These Green functions are expressed as real-space GFs in a finite cluster, i.e., for a finite number of unit cells in each layer, using lattice Fourier transformation. (iii) Regarding the STM tip as a local perturbation (loosely speaking a "defect" or "impurity"), the STM tip is eventually introduced by solving the Dyson equation for the defect potentials (that form the STM tip) in the cluster. Hence, translational invariance is lost. (iv) The conductance in the finite cluster around the STM tip is computed from the GFs obtained in step (iii).

The transformation from reciprocal to configurational space is necessary because the conductance is obtained for a tunnel junction with a single STM tip (no translational invariance). In contrast, a supercell approach computes in reciprocal space the conductance of infinitely repeated cells, each containing a STM tip. Both approaches become equivalent in the limit of infinitely large supercells.

B. KKR Green functions

The following derivations and considerations rely heavily on KKR theory. For brevity, the reader is referred to Refs. 38–40 and 30 for details. A brief introduction to typical layer KKR algorithms is given in Ref. 41.

For simplicity we restrict ourselves to the case of one atom per layer unit cell. It is straightforward to extend the theory to more atoms per cell. Note that in layer KKR (LKKR) method all layers have identical sets $\{\boldsymbol{R}^i\}$ of translation vectors, so these need not be indicated by a layer index. In the following, layers and cells are denoted by uppercase and lower-case letters, respectively. Further, the complex "energy" z at which the GFs are evaluated is dropped.

The starting point is a system that is translationally invariant parallel to the layers, that is, it has two-dimensional (2D) periodicity (no STM tip). Hence, the electronic states are characterized by the in-plane wave vector $\boldsymbol{k}_\parallel$. A KKR Green function G comprises two parts, a single-site part and a multiple-scattering part. The compact form of the single-site part is explicitly given by

$$\sum_\Lambda \langle \boldsymbol{r}_<^{0I}|Z_\Lambda^{R0I}\rangle\langle J_\Lambda^{L0I}|\boldsymbol{r}'^{\,0I}_>\rangle \equiv \sum_\Lambda \begin{cases} \langle \boldsymbol{r}^{0I}|Z_\Lambda^{R0I}\rangle\langle J_\Lambda^{L0I}|\boldsymbol{r}'^{\,0I}\rangle, & r^{0I} < r'^{0I}, \\ \langle \boldsymbol{r}^{0I}|J_\Lambda^{R0I}\rangle\langle Z_\Lambda^{L0I}|\boldsymbol{r}'^{\,0I}\rangle, & r^{0I} > r'^{0I}, \end{cases} \tag{1}$$

where $\boldsymbol{r}^{0I}$ is a vector within unit cell 0 of layer I. $\boldsymbol{r}_<^{0I}$ ($\boldsymbol{r}_>^{0I}$) denotes the smaller (larger) of $\boldsymbol{r}^{0I}$ and $\boldsymbol{r}'^{0I}$. The spin-angular multi-indices Λ comprise the angular momentum and spin quantum numbers, e.g., $\Lambda=(\kappa\mu)$ in the relativistic case[42,43] or $\Lambda=(lm\sigma)$ in the nonrelativistic case. $|Z_\Lambda^{R0I}\rangle$ and $|J_\Lambda^{R0I}\rangle$ are right-hand-side (RHS) (superscript R) regular and irregular scattering solutions of the (muffin-tin) potential located in cell 0 of layer I, respectively. The corresponding LHS scattering solutions are superscribed by L.[44]

The propagation of an electron from cell 0 in layer J to cell 0 in layer I is mediated by the scattering-path operator, with matrix elements $\tau_{\Lambda\Lambda'}^{0I;0J}$. It accounts for all scattering paths within the system. The complete GF then reads

$$G(\boldsymbol{r}^{0I},\boldsymbol{r}'^{\,0J};\boldsymbol{k}_\parallel) = \sum_{\Lambda\Lambda'} \langle \boldsymbol{r}^{0I}|Z_\Lambda^{R0I}\rangle \tau_{\Lambda\Lambda'}^{0I;0J}(\boldsymbol{k}_\parallel)\langle Z_{\Lambda'}^{L0J}|\boldsymbol{r}'^{\,0J}\rangle - \sum_\Lambda \langle \boldsymbol{r}_<^{0I}|Z_\Lambda^{R0I}\rangle\langle J_\Lambda^{L0I}|\boldsymbol{r}'^{\,0I}_>\rangle \delta^{0I;0J}. \tag{2}$$

The Kronecker δ means $\delta^{iI;iJ}=\delta_{ij}\delta_{IJ}$. Note that the GF obeys the Bloch theorem,

$$G(\boldsymbol{r}^{iI},\boldsymbol{r}'^{\,0J};\boldsymbol{k}_\parallel) = e^{i\boldsymbol{k}_\parallel\cdot\boldsymbol{R}^i} G(\boldsymbol{r}^{0I},\boldsymbol{r}'^{\,0J};\boldsymbol{k}_\parallel), \tag{3}$$

for any translation vector of the layer lattice. $\boldsymbol{R}^i$ is the translation vector from cell 0 to cell i, and $\boldsymbol{r}^{iI}=\boldsymbol{r}^{0I}+\boldsymbol{R}^i$.

To shorten the notation, scattering solutions and scattering-path operators are combined into vectors and matrices indexed by Λ,

$$(\boldsymbol{Z}^{R0I})_\Lambda \equiv |Z_\Lambda^{R0I}\rangle, \tag{4a}$$

$$(\boldsymbol{Z}^{L0I})_{\Lambda} \equiv \langle Z_{\Lambda}^{L0I}|, \tag{4b}$$

$$[\boldsymbol{\tau}^{0I;0J}(\boldsymbol{k}_{\parallel})]_{\Lambda\Lambda'} \equiv \tau_{\Lambda\Lambda'}^{0I;0J}(\boldsymbol{k}_{\parallel}). \tag{4c}$$

Note that $\boldsymbol{Z}^{R0I}$ ($\boldsymbol{Z}^{L0I}$) is a column (row) vector. Hence, Eq. (2) becomes

$$\boldsymbol{G}^{0I;0J}(\boldsymbol{k}_{\parallel}) = \boldsymbol{Z}^{R0I}\boldsymbol{\tau}^{0I;0J}(\boldsymbol{k}_{\parallel})\boldsymbol{Z}^{L0J} - \boldsymbol{Z}^{R0I}\boldsymbol{J}^{L0I}\delta^{0I;0J}. \tag{5}$$

Having determined the reciprocal-space GF of the translationally invariant system, it is transformed into real-space representation using the lattice Fourier transformation,

$$\boldsymbol{\tau}^{iI;jJ} = \frac{1}{\Omega}\int_{2\mathrm{BZ}} e^{i\boldsymbol{k}_{\parallel}\cdot(\boldsymbol{R}^i-\boldsymbol{R}^j)}\boldsymbol{\tau}^{0I;0J}(\boldsymbol{k}_{\parallel})d^2k_{\parallel}. \tag{6}$$

Ω is the area of the two-dimensional Brillouin zone (2BZ). The inverse Fourier transformation is given by

$$\boldsymbol{\tau}^{0I;0J}(\boldsymbol{k}_{\parallel}) = \frac{1}{T}\sum_{ij} e^{-i\boldsymbol{k}_{\parallel}\cdot(\boldsymbol{R}^i-\boldsymbol{R}^j)}\boldsymbol{\tau}^{iI;jJ}, \tag{7}$$

where T is the order of the translation group of the layer lattice. The real-space GF then reads

$$\boldsymbol{G}^{iI;jJ} = \boldsymbol{Z}^{R0I}\boldsymbol{\tau}^{iI;jJ}\boldsymbol{Z}^{L0J} - \boldsymbol{Z}^{R0I}\boldsymbol{J}^{L0I}\delta^{iI;jJ} \tag{8}$$

and obeys

$$\boldsymbol{G}^{(i+1)I;(j+1)J} = \boldsymbol{G}^{iI;jJ} \tag{9}$$

due to 2D translational invariance.

In the final step of the computation of the GF, the STM tip is introduced. If we consider the STM tip as a local perturbation (i.e., a defect or an impurity), it alters the scattering potentials in a finite region in the vicinity of the tip and, hence, breaks the translational invariance parallel to the layers. Note in particular that the potentials of the leads, i.e., far away from the tunnel barrier, remain unchanged. Thus, the defect region, denoted by D, comprises a finite set of cell (l) and layer (L) indices (D=$\{lL\}$ is located between L and R, all regions being disjunct). The Green function $\tilde{G}$ of the system with STM tip is obtained from the Dyson equation,

$$\tilde{G} = G + G\Delta V\tilde{G}, \tag{10}$$

where ΔV is the potential of the perturbation (quantities of systems with the STM tip are decorated by a tilde). This equation translates in the KKR formalism to

$$\tilde{\boldsymbol{G}}^{iI;jJ} = \boldsymbol{G}^{iI;jJ} + \sum_{lL\in\mathsf{D}} \boldsymbol{G}^{iI;lL}(\tilde{\boldsymbol{t}}^{lL} - \boldsymbol{t}^{lL})\tilde{\boldsymbol{G}}^{lL;jJ}, \tag{11}$$

which can be solved exactly.[45] $\tilde{\boldsymbol{t}}^{lL}$ and $\boldsymbol{t}^{lL}$ are the single-site scattering matrices of the systems with and without STM tip, respectively. In contrast to Eq. (8), the scattering solutions in $\tilde{G}$ carry a cell index because the potentials, the scattering solutions, and hence the single-site scattering matrices, depend on the cell,

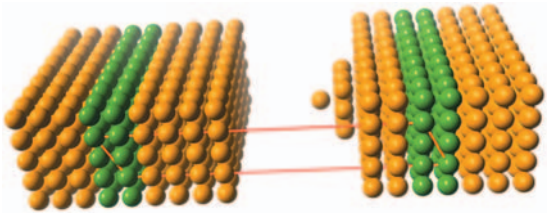

FIG. 1. (Color) Schematic representation of a STM. The left part shows the sample electrode, with the decoupling region L in green. The STM tip with its lead and its decoupling region R (also in green) is shown on the right. The closed-path summations in Eq. (19) are performed over all pairs of sites in the decoupling regions. One such closed path is shown in red. The site potentials of the decoupled and the coupled systems differ only in the two decoupling regions.

$$\tilde{\boldsymbol{G}}^{iI;jJ} = \tilde{\boldsymbol{Z}}^{RiI}\tilde{\boldsymbol{\tau}}^{iI;jJ}\tilde{\boldsymbol{Z}}^{LjJ} - \tilde{\boldsymbol{Z}}^{RiI}\tilde{\boldsymbol{J}}^{LiI}\delta^{iI;jJ}. \tag{12}$$

Eventually, the Green functions $\tilde{\boldsymbol{G}}$ for the decoupled and the coupled systems are used to compute the conductance of the STM.

C. Computation of the conductance

For the computation of the conductance of the STM, Landauer-Büttiker theory is applied. Within the electron-counting picture of transport, the conductance C of the STM junction is obtained from the transmission probabilities of all scattering channels incoming in one lead and outgoing in the other lead,[18]

$$C(V) = G_0\Theta(V), \tag{13}$$

where V is the applied bias voltage. The conductance quantum $G_0=e^2/h$ is the inverse von Klitzing constant (i.e., the quantum of resistance, $R_K\approx 25.8\ \mathrm{k}\Omega$). The total transmittance $\Theta(V)$ comprises the transmission probabilities in the "energy window of tunneling" opened by V.[46] For zero bias voltage ($V=0$, linear response), which is the case considered in this paper, only the transmittance at the common Fermi energy E_F of the two leads needs to be considered. Since the energy is fixed in the following, it is dropped in the equations.

The transmission probabilities can be computed from the GFs of a system in which the tunnel barrier is first decoupled from the leads and subsequently coupled to the leads. Within a tight-binding approach, the decoupling can be achieved by setting the hopping matrix elements between barrier and leads to zero.[47,48] Or an "impermeable membrane" between the two leads could be erected.[49] In the KKR approach, where the scattering potentials can easily be accessed, the decoupling can be achieved by erecting high potential walls of sufficiently large width between leads and tunnel barrier.[37] Although a residual coupling remains, tuning the height and width of the potential walls allows conductances to be obtained as accurately as in other sophisticated KKR approaches.[50]

The decoupling regions in which the potential walls are erected are denoted by L and R (Fig. 1). The real-space

Green function of the system with the tunnel barrier decoupled from the leads is given by (subscript "dc")

$$\tilde{\boldsymbol{G}}_{\mathrm{dc}}^{iI;jJ} = \tilde{\boldsymbol{Z}}_{\mathrm{dc}}^{RiI} \tilde{\boldsymbol{\lambda}}^{iI;jJ} \tilde{\boldsymbol{Z}}_{\mathrm{dc}}^{LjJ} - \tilde{\boldsymbol{Z}}_{\mathrm{dc}}^{RiI} \tilde{\boldsymbol{J}}_{\mathrm{dc}}^{LiI} \delta^{iI;jJ}, \tag{14}$$

with scattering-path operator $\tilde{\boldsymbol{\lambda}}$. Analogously, that of the coupled system (subscript "c") reads

$$\tilde{\boldsymbol{G}}_{c}^{iI;jJ} = \tilde{\boldsymbol{Z}}_{c}^{RiI} \tilde{\boldsymbol{\mu}}^{iI;jJ} \tilde{\boldsymbol{Z}}_{c}^{LjJ} - \tilde{\boldsymbol{Z}}_{c}^{RiI} \tilde{\boldsymbol{J}}_{c}^{LiI} \delta^{iI;jJ}, \tag{15}$$

with scattering-path operator $\tilde{\boldsymbol{\mu}}$.

For a translationally invariant system (e.g., a planar tunnel junction; cell index in principle unnecessary) the transmittance $\Theta(\boldsymbol{k}_{\parallel})$ at a particular wave vector can be obtained from

$$\Theta(\boldsymbol{k}_{\parallel}) = \sum_{IJ \in \mathsf{L}} \sum_{KL \in \mathsf{R}} \Theta^{IJ;KL}(\boldsymbol{k}_{\parallel}), \tag{16}$$

with

$$\Theta^{IJ;KL}(\boldsymbol{k}_{\parallel}) = \Delta \boldsymbol{t}^{0I} [\boldsymbol{\lambda}^{0I;0J}(\boldsymbol{k}_{\parallel}) - \boldsymbol{\lambda}^{0J;0I}(\boldsymbol{k}_{\parallel})^{\dagger}] \Delta \boldsymbol{t}^{0J\dagger} \mu^{0J;0K}(\boldsymbol{k}_{\parallel}) \times \Delta \boldsymbol{t}^{0K} [\boldsymbol{\lambda}^{0K;0L}(\boldsymbol{k}_{\parallel}) - \boldsymbol{\lambda}^{0L;0K}(\boldsymbol{k}_{\parallel})^{\dagger}] \Delta \boldsymbol{t}^{0L\dagger} \mu^{0I;0L}(\boldsymbol{k}_{\parallel})^{\dagger}. \tag{17}$$

Here, $\Delta \boldsymbol{t}^{0I}$ is the difference of the single-site scattering matrices of the coupled and the decoupled system. The summation runs over all layers in the decoupling regions L and R. Note further that the above matrices have to be obtained very close to the real energy axis, that is, the side limits of the GFs have to be considered.[38]

Equations (13), (16), and (17) are the KKR analog to the Landauer conductance formula[51]

$$C = G_0 \, \mathrm{Tr}[\mathrm{Im}(\Sigma_{\mathsf{L}}) G \, \mathrm{Im}(\Sigma_{\mathsf{R}}) G^{\dagger}], \tag{18}$$

where the Green function G propagates an electron from the right to the left lead. This is accomplished in KKR theory by the scattering-path operator (SPO) $\boldsymbol{\mu}$ in Eq. (15). The self-energies Σ_{L} and Σ_{R} account for the decoupling of the leads and the barrier. Their imaginary parts translate in the KKR approach into terms like $\Delta \boldsymbol{t}^{0I} [\boldsymbol{\lambda}^{0I;0J}(\boldsymbol{k}_{\parallel}) - \boldsymbol{\lambda}^{0J;0I}(\boldsymbol{k}_{\parallel})^{\dagger}] \Delta \boldsymbol{t}^{0J\dagger}$ [cf. Eq. (17)].

It is straightforward, using the lattice Fourier transform [Eqs. (6) and (7)], to obtain an expression for the conductance in real space. For Θ one gets

$$\Theta = \frac{1}{T} \sum_{iI;jJ \in \mathsf{L}} \sum_{kK;lL \in \mathsf{R}} \Delta \boldsymbol{t}^{iI} (\boldsymbol{\lambda}^{iI;jJ} - \boldsymbol{\lambda}^{jJ;iI\dagger}) \Delta \boldsymbol{t}^{jJ\dagger} \mu^{jJ;kK} \Delta \boldsymbol{t}^{kK} \times (\boldsymbol{\lambda}^{kK;lL} - \boldsymbol{\lambda}^{lL;kK\dagger}) \Delta \boldsymbol{t}^{lL\dagger} \mu^{iI;lL\dagger}. \tag{19}$$

The prefactor $1/T$ appears due to the translational invariance, implying that Θ is the transmittance per cell. Note further that any scattering-path operator for this system obeys $\boldsymbol{\tau}^{iI;jJ} = \boldsymbol{\tau}^{(i+1)I;(j+1)J}$. We would like point out that each term in the above sum specifies a closed path in real space (Fig. 1).

The loss of translational invariance (due to the STM tip) imposes the question of how to identify the effect of the STM tip on the conductance, as compared to that of a planar tunnel junction (PTJ). For a translationally invariant system, namely, a PTJ, one defines a transmittance per cell, as in Eq. (19). Evidently, the total transmittance is infinite due to the infinite number of cells through which the current flows. Accordingly, the total transmittance of a STM is infinite, too.

In order to identify uniquely the difference of the conductances of the STM and PTJ we proceed as follows. The sums in Eq. (19) run over the infinite number of cells in regions L and R. The real-space cluster cuts out a finite subset of the infinite cell set, denoted by C. Hence, the total transmittance of a PTJ can be expressed as

$$\Theta_{\mathrm{tot}} = \Theta(\mathsf{C}) + \Theta(\bar{\mathsf{C}}). \tag{20}$$

$\Theta(\mathsf{C})$ comprises all conductance paths that lie within C (Fig. 1), whereas $\Theta(\bar{\mathsf{C}})$ contains all other paths. With Eq. (19), one has $\Theta_{\mathrm{tot}} = T\Theta$, and both Θ_{tot} and $\Theta(\bar{\mathsf{C}})$ become infinite if the order of the translation group $T \to \infty$. For a STM one has accordingly

$$\tilde{\Theta}_{\mathrm{tot}} = \tilde{\Theta}(\mathsf{C}) + \tilde{\Theta}(\bar{\mathsf{C}}). \tag{21}$$

If the cluster C is sufficiently large (which needs to be checked by convergence tests; see Sec. III A), one has $\tilde{\Theta}(\bar{\mathsf{C}}) \approx \Theta(\bar{\mathsf{C}})$. The transmittance difference, that is, the effect of the STM tip, is then given by

$$\Delta\Theta = \tilde{\Theta}_{\mathrm{tot}} - \Theta_{\mathrm{tot}} \approx \tilde{\Theta}(\mathsf{C}) - \Theta(\mathsf{C}). \tag{22}$$

The knowledge of both $\Delta\Theta$ and Θ from Eq. (19) allows one to investigate the effects of tip-sample interaction and of electronic states localized at the STM tip. We note in passing that $\Delta\Theta$ can be calculated directly from the transmittances Θ and $\tilde{\Theta}$ of the PTJ and the STM. Another way is to express $\Delta\Theta$ in terms of the Green function of the barrier (with SPOs $\tilde{\boldsymbol{\mu}}$ and $\boldsymbol{\mu}$), since these are related by a Dyson equation for the STM tip region [similar to Eq. (11)], and use that expression in the numerical computation. In the present paper, the conductance of the STM is obtained from Eqs. (19) and (22) but for the SPOs and single-site t matrices obtained by solving the Dyson equation for the tip region, that is, with $\tilde{\boldsymbol{\lambda}}$, $\tilde{\boldsymbol{\mu}}$, etc.

D. Discussion of approximations

The proposed approach relies on the 2D lattice Fourier transformation, in order to compute the real-space KKR Green function. This implies that a 2D periodicity is inherent to the entire system, including both electrodes. In other words, each layer has to have identically shaped unit cells.

In a practical computation, several restrictions apply due to limitations of computer memory and computation time. A first problem is the accurate determination of the real-space GFs from the reciprocal-space GFs [Eqs. (6) and (8)]. Regardless of whether an equidistant $\boldsymbol{k}_{\parallel}$ mesh, for example special points,[52] or an adaptive integration method[53] is used, for a correct description of the electronic structure the number of $\boldsymbol{k}_{\parallel}$ needed is on the order of several 1000 to several 10 000 wave vectors. Note in this respect that KKR GFs have to be computed for complex energies, the imaginary part of which is chosen on the order of meV or μeV.

A second problem appears due to the finite size of the real-space cluster C. In principle, the conductance of the entire surface-tip system needs to be computed, which is obviously impossible. Thus, the summations in Eq. (19) over

L and R have to be restricted to a finite cluster C surrounding the STM tip, the size of which has to be determined by convergence tests (see also Ref. 54). A finite cluster is sufficient because in a STM the current flows almost exclusively through the STM tip ("eye of the needle") and proceeds in a cone with finite opening angle.[55–58] The other regions (which can be viewed as parts of a planar tunnel junction with a wide vacuum barrier) contribute much less to the conductance. This will be elucidated by the convergence tests presented in Sec. III A.

The Landauer-Büttiker theory assumes the transmission of Bloch states of the leads (scattering boundary conditions) computed infinitely far from the tunnel junction. Here, a third problem arises from the fact that the summation over the decoupling regions L and R in the conductance calculation is not performed infinitely far from the tunnel barrier but typically rather close to the surface of the leads (Fig. 1).[54] Thus, the conductance might be influenced by the surface electronic structure, in particular by surface states which decay slowly toward the bulk [as is, for example, the case[34] for Au(111)]. The effect of the surface electronic structure can be determined by comparing the conductances for the planar tunnel junction (without STM tip) obtained with the Bloch-wave transmission approach by MacLaren and co-workers[50] (which by construction does not include surface contributions) and the present approach.

Since the decoupling is achieved by potential walls of finite height in a finite number of layers, there remains a residual coupling which in principle can be made negligibly small. It turns out that typically a minimum of four layers with potentials of 2 Hartree height are sufficient. Note that the decoupling can be checked by computing the conductance of a bare lead, i.e., a system entirely built of a single ideal lead. In this case, the transmission probability must equal the number of scattering channels (Sharvin conductance[59]).

Another problem when implementing a new approach is to test its accuracy. For planar tunnel junctions, we have implemented the Bloch-wave transmission approach,[50] an approach based on the Kubo-Greenwood formula for the conductivity tensor,[60–62] and the present GF approach in our modular LKKR computer code.[37] It was shown for the former and latter approaches that these give almost identical results, even for complex systems (e.g., Fe/MgO/Fe with FeO interfaces).[63] The latter method[37] is the basis for the real-space STM approach presented here. The LKKR computer code was extended to deal with clusters in real space and with the Dyson equation. All these parts were cross checked with other KKR codes and tested for other computational modes (such as, for example, Bloch spectral densities and density of states).

Recently, a GF approach for the STM was implemented by Blanco *et al.* (see Ref. 20 and references therein). Although similar to the approach presented here, it relies on a slab calculation involving supercells rather than treating semi-infinite leads and a single STM tip. An advantage of that implementation is that relaxations of both the surface and the tip atoms can be taken into account. In favor of our approach, we would like to note that, in principle, relaxations can be treated as well by solving a Dyson equation for the atoms displaced from their ideal positions (see, for example, Refs. 64 and 65). This would allow to investigate the effect of tip-induced relaxations on the tunneling conductance.[66,67]

A nonequilibrium Green function approach for calculating the electronic transport of atomic-scale systems was described by Brandbyge *et al.*[68] The scattering region is defined within a finite supercell and consequently the GF matrix might not be sufficiently large to minimize interference effects. The latter are induced by the repeated images of the STM tip. However, the indisputable advantage of this method is that the charge-density matrix is clearly expressed in two parts, i.e., an equilibrium and a nonequilibrium contribution. The technique can thus be extended to multiterminal devices.

In the present work we focus on the conductance for zero bias voltage. An extension to finite bias could be performed within the framework of nonequilibrium Green functions or by assuming a heuristic voltage drop within the vacuum barrier (typically a linear dependence, as, e.g., in Refs. 46 and 69–71). Both approaches have already been applied successfully. In particular, it can be shown that a multiple-scattering theory based on nonequilibrium Green functions systematically corrects the Bardeen formalism for nonzero bias voltage.[72] The latter allows, in particular, the sample and the tip contributions to the conductance to be distinguished,[73] as opposed to the Landauer-Büttiker formalism.

E. Size and shape of the real-space cluster

A conductance calculation for a tunnel junction (either a planar or a STM junction) is computationally demanding. But if the chosen method is a real-space approach it is even more demanding. Therefore, it is desirable to reduce the number of cells in the cluster as far as possible but without perceptible loss of accuracy. Further, the shape of the cluster has to be chosen appropriately, keeping in mind the "bottleneck" picture behind the STM tip. By this means a lot of computer memory and computational time can be saved.

A cluster with rhomboidal cross section (top in Fig. 2) has two basic shortcomings. Considering the cone-shaped electron flux through the tip, cells far away from the tip position (in particular those at the corners) do not contribute significantly to the conductance and, hence, can be neglected if the cluster is sufficiently large. On the other hand, if the cluster is not large enough, important contributions may be missed, especially from cells at edge centers. These drawbacks can be overcome if the cluster accounts for the cone-shaped electron flux through the STM tip, in particular by taking a cluster with circular cross section (bottom in Fig. 2).

Another important point concerns the set of layers for which the Green functions have to be explicitly computed. In view of the above derivation (Secs. II B and II C), only a few layers in the decoupling regions (for computing the conductance) and the layers of the STM tip (for solving the Dyson equation) have to be considered.

Both improvements are implemented in our object-oriented layer KKR computer code. The sets of cells can be chosen differently for each layer. For a typical setup the total number of cells is reduced from about 1936 for the full real-

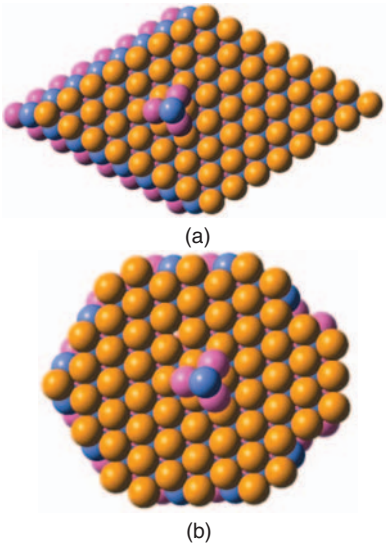

FIG. 2. (Color) Clusters with two different lateral shapes (schematic). In each layer, a cluster has either a rhomboidal (top) or a circular cross section (bottom). The STM tip consists of four atoms. Layers appear shifted in accordance with the …*ABCABC*… stacking in the [111] direction of the fcc parent lattice and are distinguished by color.

space cluster to 264 for the improved one. This corresponds to a reduction of computer memory from about 25 to about 1.2 Gbytes.

F. Computation

The electronic properties of the tunnel junctions discussed in Sec. III were obtained within the local spin-density approximation to density-functional theory, using a multicode approach. The *ab initio* calculations are performed with the KKR code HUTSEPOT, details of which can be found in Refs. 74–77. The generated self-consistent potentials serve as input for the conductance calculations, using the spin-polarized relativistic layer KKR code OMNI2K. The latter is focused on the computation of electron spectroscopy, rather than on performing *ab initio* calculations. It solves the Dirac equation for the single-site problem, and spin-orbit coupling is included in both the electronic-structure and the transport calculations.

Self-consistent computations were performed for a planar tunnel junction comprising two semi-infinite Au(111) electrodes separated by four layers of vacuum (see inset in Fig. 7). The potential in the vacuum region is described by muffin-tin spheres (empty sites), as for Au atoms. These computations proceeded like those for the bare Au(111) surface, details of which can be found in Ref. 36. However, tunneling through a junction imposes additional problems, so more computational details are in order.

The crystal potentials are represented in the atomic sphere approximation (ASA), in which the atomic spheres associated with each scatterer fill the configurational space (real space) but overlap. Although the crystal potential is in principle described better than in the muffin-tin approximation (MTA) with nonoverlapping spheres, the overlap results in an incorrect (additional) scattering of the electrons. To overcome this problem, we used the so-called ASAMT approach.[78] This approach corrects for the additional scattering contributions. It relies on overlapping atomic spheres in the calculation of the kinetic energy, similar to the ASA. However, a shape correction is utilized which has the same form as in the MTA treatment of the interstitial. The inter-site Coulomb energy is evaluated using the Madelung energy as computed in the MTA while the on-site Coulomb energy is calculated using the ASA. The Madelung potential is obtained by a two-dimensional Ewald procedure[79] for semi-infinite lattices with proper boundary conditions (that is, two semi-infinite bulk materials which represent the electrodes). If the two leads are made of different materials, the Madelung potential is adjusted to an electrostatic dipole barrier which is related to the associated Fermi levels.

The potentials are spherically symmetric within the atomic spheres in both the electrodes and the vacuum barrier region. This shape approximation might result in an inaccurate description of the surface electronic structure, in particular at the STM tip (see, e.g., Ref. 80). Although implemented in both KKR codes, a full-potential approximation was not applied due to a substantial increase of computation time. We would like to recall that even spherically symmetric potentials allow accurate description of the electronic structure of strongly corrugated surfaces, such as of the ordered surface alloy Bi/Ag(111).[81]

The STM tip consists of four Au atoms placed in a tetrahedron on top of one of the Au(111) surfaces of the PTJ (Fig. 2 and insets in Fig. 7). The positions of the tip atoms are those of the fcc parent lattice, with the apex atom supported by three atoms (we note in passing that the tip shape influences the differential conductance; e.g. Refs. 73 and 82). The tip-sample distance is two layers (i.e., 4.86 Å; PTJ, four layers), resulting in a much larger conductance than for the PTJ. Based on the self-consistent calculation for the PTJ, the potentials of the STM junction were obtained by solving the Dyson equation in a 3D cluster around the tip. The herringbone reconstruction of the Au(111) surface is not considered.[83]

Self-consistent calculations have to be performed only for the coupled systems. The potentials of the decoupling walls in L and R (green in Fig. 1) can be taken as constant in the muffin-tin spheres. Since scattering boundary conditions apply, the calculation is performed for the tunnel junction embedded between the semi-infinite leads.[37]

The results of the self-consistent electronic-structure calculations serve as input for the conductance calculations. Several methods for computing the ballistic conductance are implemented in our KKR codes, allowing validation of the proposed approach. Further, the dependence of the conductance on free parameters (e.g., the number of $\boldsymbol{k}_{\parallel}$ used in the 2BZ integration) could be checked. All results presented in Sec. III were obtained for zero bias and for real-space clusters with a circular cross section (Sec. II E). The regions L and R were chosen four layers wide, covering the outermost Au surface layers, and found to provide sufficient decoupling with potential walls of 2 Hartree height. The entire junction comprises 16 layers in total, six for each Au lead and four for the tip-vacuum region. Summations over the 2BZ involve about 10 000 wave vectors.

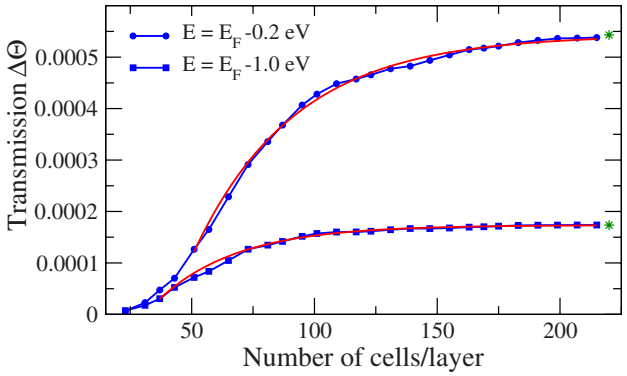

FIG. 3. (Color online) Transmittance $\Delta\Theta$ of a Au(111) STM junction versus number of cells per layer in regions L and R [cf. Eqs. (19) and (22)] for two energies $E=E_F-0.2$ eV (circles) and $E_F-1.0$ eV (squares). Both curves are fitted to $\Delta\Theta(x)=\Delta\Theta_\infty - a\exp(-bx)$ (red), where x is the number of cells per layer. Both values of $\Delta\Theta_\infty$ are represented by green asterisks.

III. APPLICATION TO TUNNEL JUNCTIONS WITH Au(111) ELECTRODES

In order to show the reliability of the proposed approach for calculating the conductance of a STM, we choose tunnel junctions with Au(111) electrodes as an example. Besides a planar tunnel junction, which comprises the two Au(111) electrodes and four layers of vacuum as tunnel barrier, a STM with Au(111) electrodes and a four-atom tip (tetrahedron) is investigated (see insets in Fig. 7).

A. Convergence with respect to cluster size

An important approximation in the proposed method is that the conductance is computed in a finite-sized cluster C around the STM tip [Eq. (19) and Sec. II D]. The method has to be rendered unusable if the conductance does not converge with increasing number of cells within the layers. Therefore, the convergence of the transmittance has to be checked by increasing the lateral size of the real-space cluster C.

Two energies are considered. The first, 0.2 eV below the Fermi level (E_F), is within the energy range covered by the L gap surface state present at the bare Au(111) surface. Note that this surface state has a band minimum at $E_F-0.5$ eV and shows parabolic dispersion.[84] The other energy, 1.0 eV below E_F, accounts only for Au bulk states. For both energies, the transmittance $\Delta\Theta$ [Eq. (22)] plotted versus number of cells within a layer of the tunnel junction starts to increase almost linearly and saturates at about 190 cells per layer (Fig. 3). In order to find the converged values $\Delta\Theta_\infty$ of $\Delta\Theta$, the curves are fitted to $\Delta\Theta(x)=\Delta\Theta_\infty-a\exp(-bx)$ (red in Fig. 3), where x is the number of cells per layer. From the fits we obtain $\Delta\Theta_\infty=0.000\,543$ and $0.000\,173$ for $E_F-0.2$ eV and $E_F-1.0$ eV, respectively (indicated by green asterisks). Our finding corresponds nicely to the trend observed in Ref. 54.

The trend can be understood by considering the cone-shaped flux through the STM tip as follows. Areas far apart from the STM tip can be regarded as planar tunnel junctions, the electrodes of which are separated by four vacuum layers. In contrast, the tip-sample separation at the apex atom of the STM tip is only two layers. Hence, the contribution of the area around the STM tip to the conductance is much larger than that of the remainder of the system (although its area is much larger). That can be understood by the exponential decrease of the transmittance through a tunnel barrier with increasing electrode separation. Due to scattering at the tip atoms, the current flows in a cone with moderate opening angle, the cone being centered about the apex atom of the tip. (A similar behavior is found in quantum point contacts.[55]) For a converged conductance, the summation over the cells in L and R [Eq. (19)] has to cover at least the cross section of the cone.

B. Effect of the STM tip on the sample

An advantage of the present approach is that the tip-sample interaction is fully accounted for by considering the electronic structure of the entire tunnel junction, as opposed to the Tersoff-Hamann and transfer-Hamiltonian approaches. Therefore, we consider in the following the effect of the STM tip on the electronic structure of the sample. Tip-induced relaxation, which might be important,[85] is neglected so far.

The effect of the STM tip on the electronic structure can be investigated by means of the local density of states (LDOS),

$$N^{iI}(E) = -\frac{1}{\pi}\lim_{\eta\to+0}\ \mathrm{Im}\,\mathrm{Tr}\,G^{iI;iI}(E+\mathrm{i}\,\eta), \tag{23}$$

where iI specifies the cell (atom) i in layer I. The spatial integration included in the trace Tr is over the corresponding cell. The LDOS induced by the STM tip is then

$$\Delta N^{iI}(E) = \tilde{N}^{iI}(E) - N^{iI}(E), \tag{24}$$

that is, the LDOS difference between the systems with and without the STM tip.

The induced LDOS of the surface layer of the sample is shown in Fig. 4. In the outer region, the LDOS is that of the bare surface (no STM tip), depicted in blue. In the center, the STM tip induces an increased LDOS that reflects the three-fold symmetry of the tip (note the tetrahedral arrangement of tip atoms). The induced density is, however, very small (about 5.5×10^{-5} states/Hartree) and can be neglected for the chosen system. The tip-sample interaction may become significant for reduced tip-sample distances or for transition metal surfaces (instead of noble metal surfaces).

The induced local density of states of the STM tip is displayed in Fig. 5. In the layer that contains the apex atom, the LDOS is almost zero everywhere (blue in the top panel), except at the apex atom itself. The supporting layer comprises three Au atoms that result in a triangular-shaped distribution (middle panel). This shape is maintained in the surface layer of the tip electrode (bottom panel), with an increase of about 2 states/Hartree as compared to that of the bare surface (dark blue). Note that this increase is much larger than that induced on the sample electrode (Fig. 4) due

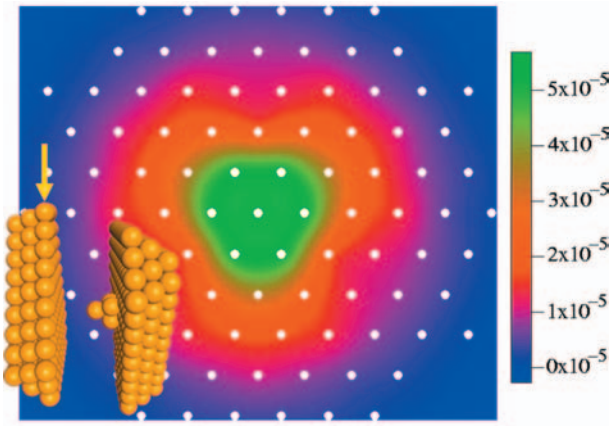

FIG. 4. (Color) Effect of the STM tip on the electronic structure of the sample. The induced local density of states $\Delta N^{iI}(E)$ of the outermost surface layer of the sample electrode is shown as color scale ($E=E_F-0.48$ eV). The LDOSs of the individual sites are interpolated to achieve a smooth color gradient. The scale bar on the right is in states per Hartree. White dots represent lattice sites; the surface layer is marked by the yellow arrow.

to direct contact with the STM tip. It turns out that the effect of the STM tip on the electronic structure is strongly localized laterally, thereby supporting the cone-shaped flux argument given above.

C. Effect of the STM tip on the conductance

Localized electronic states, such as surface states or states at the STM tip, can play a crucial role in tunneling. Depending on the underlying theory of tunneling, these either contribute to the conductance (e.g., in transfer-Hamiltonian approaches) or do not contribute [e.g., in the Landauer-Büttiker (LB) approach for a PTJ]. A reason is that the LB theory describes coherent tunneling whereas the Bardeen approach describes incoherent tunneling (a comparison of both approaches for planar tunnel junctions is given in Ref. 86). In this section, we investigate the effect of the STM tip on the conductance by comparing it to that of a planar tunnel junction, using identical setups and free parameters in the calculations.

Due to the 2D translational invariance in a planar tunnel junction, the in-plane wave vector $\boldsymbol{k}_\parallel$ is a good quantum number and, hence, is conserved in the tunnel process. Within LB theory, the total transmittance through the device is given by the sum of the transmission probabilities for each $\boldsymbol{k}_\parallel$ in the 2BZ [Eqs. (16) and (17)]. Since the wave vector before the transmission, $\boldsymbol{k}_\parallel$, equals that after the transmission, $\boldsymbol{k}'_\parallel$, the tunneling can be regarded as specular. Surface states cannot show up because these are orthogonal to the Bloch states in the leads.[87,88]

To observe surface states in the conductance, a mechanism is needed that enables scattering from the surface state into lead-Bloch states and vice versa. Such a mechanism is, for example, provided by structural disorder or (inelastic) scattering at magnons or phonons. A further mechanism is inherent to the STM: the presence of the tip (which can be regarded as a defect) breaks the 2D translational invariance,

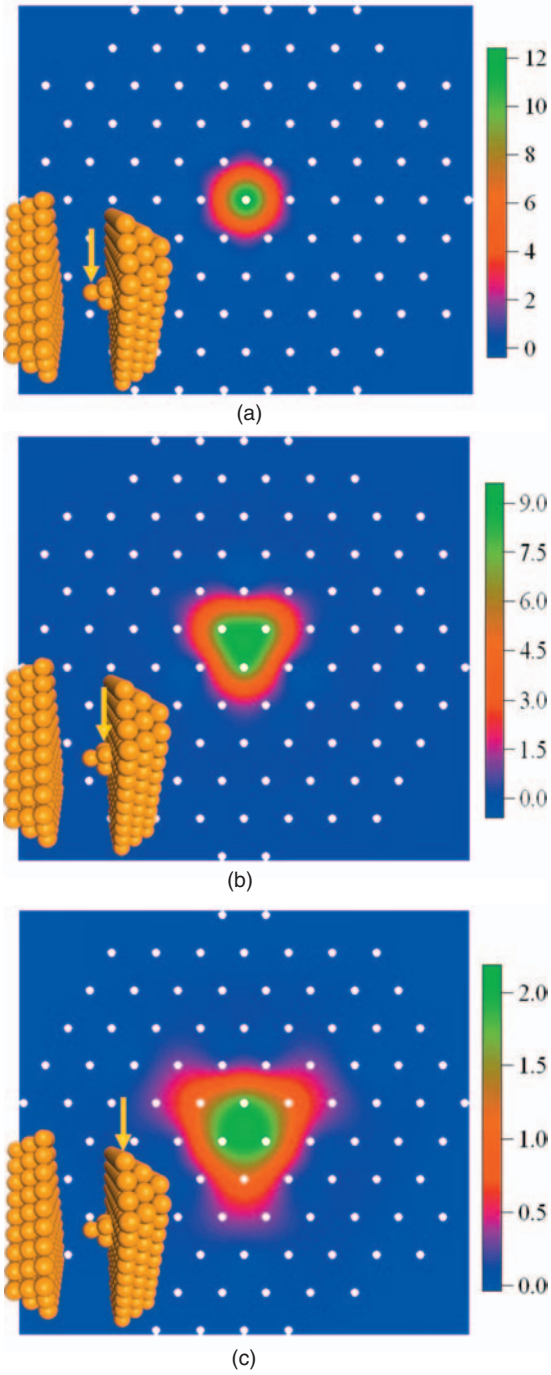

FIG. 5. (Color) Electronic structure of the STM tip. The local density of states $\Delta N^{iI}(E)$ of tip-electrode layers containing the apex tip atom (top), the supporting atoms (middle), and those of the outermost surface layer (bottom) are shown as color scale (in states per Hartree). Yellow arrows mark the respective layers. Details as for Fig. 4.

allowing the tunneling of scattering channels (Bloch states) via surface states [see, e.g., Refs. 46 and 69 for Co(0001)]. Since the wave vector of the Bloch state before the transmission, $\boldsymbol{k}_\parallel$, does not equal that after the transmission, $\boldsymbol{k}'_\parallel$, the tunneling can be regarded as diffusive.

However, diffusive scattering involves a passage (at least) three times through the vacuum barrier: an incoming electron

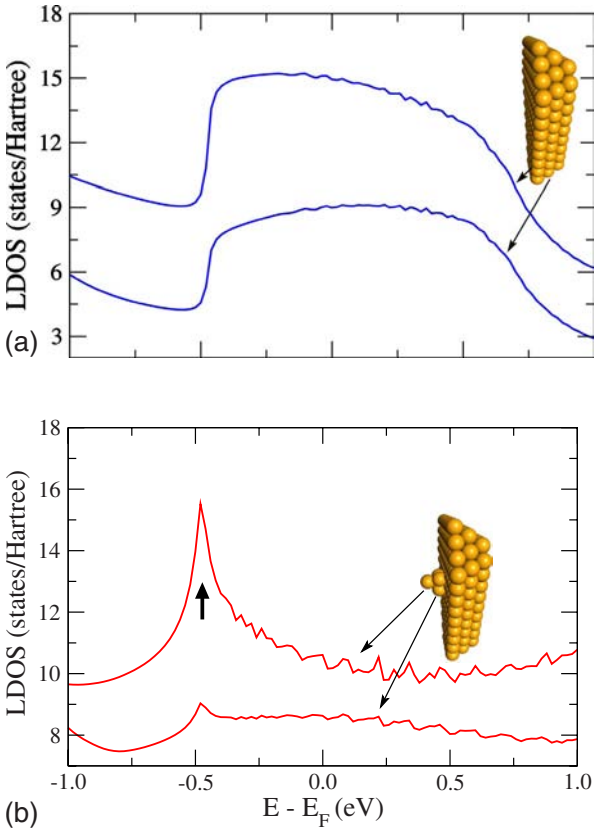

FIG. 6. (Color online) Local density of states of the Au(111) surface (top) and the STM tip (bottom). The former, showing the LDOS of a surface (top spectrum) and a subsurface atom (bottom spectrum, as indicated), is computed for wave vectors close to the center of the 2BZ to emphasize the L gap surface state in Au(111). The latter depicts the LDOS of the apex atom (top spectrum) and of a supporting atom (bottom spectrum, as indicated) of the STM tip. A cusplike feature due to an electronic state localized at the tip apex is marked by a vertical arrow. Spectra are offset by 3 states/Hartree for clarity.

is scattered at the tip, propagates through the barrier into the surface states, and propagates back to the tip, where it is scattered into an outgoing Bloch state which has to pass the barrier again to become outgoing in the other electrode. Consequently, surface states do not show up in the conductance for large tip-sample distances but can contribute significantly for small separations (note the exponential decrease of the transmittance with increasing electrode separation). Within this respect, we expect a very weak effect of the L gap surface state on the conductance, as is also suggested by the weak tip-sample interaction (Fig. 4). A more important effect is expected from electronic states located at the tip (Fig. 5). Here, the passage of an electron through the barrier takes place at least once and, hence, the contribution of tip states to the conductance is expected to be much larger than that of the surface states.

The local density of states of the Au(111) surface is shown in Fig. 6 (top). To make the L gap state clearly visible, the $\boldsymbol{k}_\parallel$ summation was restricted to the central part of the 2BZ [$|\boldsymbol{k}_\parallel| \leq 0.12 a_0^{-1}$ (Bohr radii)]. The surface state shows almost

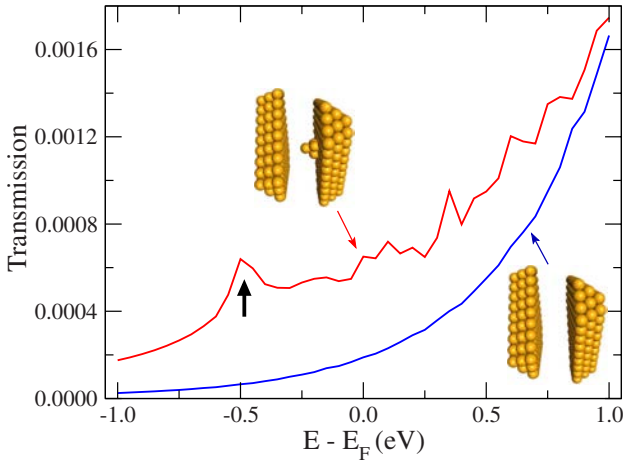

FIG. 7. (Color online) Transmittances of Au(111) tunnel junctions. The transmittances of the planar tunnel junction (lower curve; multiplied by a factor of 20 for better comparison) and the tip-induced transmittance ($\Delta\Theta$, upper curve) versus energy are shown. The increased transmittance due to an electronic state localized at the tip apex is marked by a vertical arrow (cf. Fig. 6).

the constant LDOS of a 2D free electron gas, as expected. Details on this state can be found in Ref. 36 (and references therein). [The small oscillations in the LDOS are an artifact of the finite number of special $\boldsymbol{k}_\parallel$ points used in the 2BZ integration[52] in conjunction with a tiny imaginary part η of the energy, Eq. (23)].

The LDOS for the STM tip is shown in Fig. 6 (bottom). Here, the $\boldsymbol{k}_\parallel$ summation is performed over the entire 2BZ. A prominent contribution of the apex atom is observed as a cusplike peak at $E_F - 0.48$ eV (top spectrum). It appears at the band bottom of the L gap state of the bare surface (which is at -0.5 eV), indicating its surface-state origin. This is supported by its orbital composition which is consistent with that of the surface state. The STM tip can be viewed as a protrusion with an attractive potential which results in this localized electronic state. Its energy is hence expected to be close to the band bottom of the L gap surface state. [Additional calculations for Ag(111) support this explanation: replacing Au by Ag, the band bottom of the surface state is shifted to higher energies, and so is the tip-related electronic state.] Its spectral weight decreases rapidly toward the bulk, in particular much more rapidly than that of L gap surface state. Therefore, a significant effect on the conductance from this state is expected (see also Ref. 89).

Having considered tip-induced effects on the electronic structure of the STM junction, we now discuss the energy-resolved transmittances of the PTJ and the STM. Their difference $\Delta\Theta$ (upper curve in Fig. 7) directly shows the effect of the STM tip as compared to a planar tunnel junction. We note that the PTJ transmittance was also calculated by the Bloch-wave transmission method of MacLaren *et al.*,[37,50] showing agreement with that obtained by the real-space approach.

The transmittance of the PTJ is monotonically increasing (lower curve in Fig. 7). This behavior is expected because in the given energy range only the free-electron-like *sp* states of

Au contribute to the conductance. The increase is thus similar to that observed in tunneling of free electrons through a potential step.[90,91]

The transmittance in the PTJ is much smaller than that of the STM (upper curve in Fig. 7), which is attributed to the larger effective width of the vacuum barrier: four layers for the PTJ, two for the STM. The most striking difference, however, is the maximum in the STM transmittance at $E_F - 0.48$ eV. Both shape and energy position suggest that its origin is the electronic state localized at the STM tip (Fig. 6). We note that calculations for a Ag(111) tunnel junction produced similar results, with the main difference being a different binding energy of both the L gap surface state and the tip-induced state (as compared to Au). Summarizing, we find a significant effect of electronic states localized at the STM tip on the conductance.

IV. CONCLUDING REMARKS

A new approach for computing scanning tunneling microscopy from first principles is proposed. Within the framework of Landauer-Büttiker theory, the conductance of a scanning tunneling microscope is obtained from the transmittance of the scattering channels through the interface region (the surfaces of the electrodes and vacuum barrier including the STM tip). Tip-sample interaction is accounted for by computing the electronic structure of the entire tunnel junction. Furthermore, repeated images of the STM tip, as being present in a supercell approach, are avoided by solving the Dyson equation for the STM tip in real space (configuration space). Although formulated in multiple-scattering theory (the layer Korringa-Kohn-Rostoker approach), the proposed approach can be implemented in any Green-function method for electronic-structure calculations.

The applicability of the method is proven by investigating the effect of the STM tip on the conductance of Au(111) tunnel junctions. The conductance of a STM is compared to that of a corresponding planar tunnel junction. It is found that electronic states localized in the STM tip contribute significantly to the conductance, showing that diffusive tunnel processes are accounted for in the presented approach.

Finally, we would like to point out a difference from the Tersoff-Hamann model. In the TH model, an increase of the tip-sample distance gives stronger emphasis to surface-state contributions to the conductance, while bulk-state contributions become reduced. The very reason is that generally the local density of surface states extends more into the vacuum barrier than that of bulk states. Within the present Landauer-Büttiker-based approach, however, an increase of the tip-sample distance reduces surface-state contributions because the probability of diffusive scattering due to the STM tip decreases with respect to the probability of specular scattering. This can be explained as follows. The scattering channels are orthogonal to the localized states (surface states or tip states). As a consequence, the latter states do not contribute to the conductance if there is no means to couple them to the scattering channels. This is in particular the case for planar tunnel junctions (note that the in-plane wave vector is conserved for these systems). In a STM, however, the tip itself provides a means to scatter the channels in and out of the localized states. For a surface state to contribute, an incoming electron has to pass at least three times the vacuum barrier and scattered twice at the STM tip. Hence, the transmission amplitude is expected to be much smaller than for electrons that pass the vacuum barrier only once. Consequently, the decrease of the surface-state contributions with increasing tip-sample distance are not an artifact of the proposed approach but are inherent in the Landauer-Büttiker theory. It appears worth investigation in the future, especially by comparing theoretical results obtained by both approaches with experimental data.

The method can also be applied to nanowires and atomic point contacts, provided the electric current flows through a bottleneck (as opposed to a PTJ). Based on Green functions, substitutional disorder can be treated within the inhomogeneous coherent-potential approximation,[30,40,45] hence avoiding averaging over configurations in a supercell approach. Problems worth investigation in the future are substitutional disorder in the interface region and magnetic disorder in a magnetic tunnel junction, for example in the disordered local moment picture (e.g., Ref. 92). Since the method is implemented in a spin-polarized relativistic layer KKR code, spin-dependent conductances can also be computed, allowing investigation of spin-resolved scanning tunneling microscopy and tunnel magnetoresistances. Further, due to the inclusion of spin-orbit coupling, it is straightforward to study noncollinear magnetic configurations which might show up at the STM tip and in nanowires.

*Present address: CSMD, Oak Ridge National Laboratory, Oak Ridge, Tennessee 37831, USA. sahakk@ornl.gov

[1] G. Binnig and H. Rohrer, Rev. Mod. Phys. **59**, 615 (1987).
[2] F. Besenbacher, Rep. Prog. Phys. **59**, 1737 (1996).
[3] *Scanning Tunneling Microscopy III. Theory of STM and Related Scanning Probe Methods*, edited by R. Wiesendanger and H.-J. Güntherodt (Springer, Berlin, 1993).
[4] J. Tersoff and D. R. Hamann, Phys. Rev. Lett. **50**, 1998 (1983).
[5] J. Tersoff and D. R. Hamann, Phys. Rev. B **31**, 805 (1985).
[6] J. Bardeen, Phys. Rev. Lett. **6**, 57 (1961).
[7] N. Papanikolaou, B. Nonas, S. Heinze, R. Zeller, and P. H. Dederichs, Phys. Rev. B **62**, 11118 (2000).
[8] M. Bode and R. Wiesendanger, in *Magnetic Microscopy of Nanostructures*, edited by H. Hopster and H. P. Oepen (Springer, Berlin, 2005), p. 203.
[9] S. Heinze, R. Abt, S. Blügel, G. Gilarowski, and H. Niehus, Phys. Rev. Lett. **83**, 4808 (1999).
[10] S. Heinze, G. Bihlmayer, and S. Blügel, Phys. Status Solidi A **187**, 215 (2001).
[11] D. Wortmann, S. Heinze, P. Kurz, G. Bihlmayer, and S. Blügel,

Phys. Rev. Lett. **86**, 4132 (2001).
[12] M. Bode, S. Heinze, A. Kubetzka, O. Pietzsch, X. Nie, G. Bihlmayer, S. Blügel, and R. Wiesendanger, Phys. Rev. Lett. **89**, 237205 (2002).
[13] M. Bode, A. Kubetzka, S. Heinze, O. Pietzsch, R. Wiesendanger, M. Heide, X. Nie, G. Bihlmayer, and S. Blügel, J. Phys.: Condens. Matter **15**, S679 (2003).
[14] K. von Bergmann, M. Bode, A. Kubetzka, M. Heide, S. Blügel, and R. Wiesendanger, Phys. Rev. Lett. **92**, 046801 (2004).
[15] W. A. Hofer and J. Redinger, Philos. Mag. B **78**, 519 (1998).
[16] W. A. Hofer, Prog. Surf. Sci. **71**, 147 (2003).
[17] W. A. Hofer, J. Redinger, A. Biedermann, and P. Varga, Surf. Sci. **482-485**, 1113 (2001).
[18] Y. Imry and R. Landauer, Rev. Mod. Phys. **71**, S306 (1999).
[19] K. S. Thygesen and K. W. Jacobsen, Phys. Rev. B **72**, 033401 (2005).
[20] J. M. Blanco, C. González, P. Jelínek, J. Ortega, F. Flores, and R. Pérez, Phys. Rev. B **70**, 085405 (2004).
[21] W. H. Butler, Phys. Rev. B **31**, 3260 (1985).
[22] P. Weinberger, P. Levy, J. Banhart, L. Szunyogh, and B. Újfalussy, J. Phys.: Condens. Matter **8**, 7677 (1996).
[23] K. Carva, I. Turek, J. Kudrnovský, and O. Bengone, Phys. Rev. B **73**, 144421 (2006).
[24] R. Zeller, Phys. Rev. B **55**, 9400 (1997).
[25] R. Zeller, P. H. Dederichs, B. Újfalussy, L. Szunyogh, and P. Weinberger, Phys. Rev. B **52**, 8807 (1995).
[26] K. Wildberger, R. Zeller, and P. H. Dederichs, Phys. Rev. B **55**, 10074 (1997).
[27] J. Schwitalla and B. L. Györffy, J. Phys.: Condens. Matter **10**, 10995 (1998).
[28] N. Y. Moghadam, G. M. Stocks, B. Újfalussy, W. A. Shelton, A. Gonis, and J. S. Faulkner, J. Phys.: Condens. Matter **11**, 5505 (1999).
[29] I. Turek, J. Kudrnovský, V. Drchal, L. Szunyogh, and P. Weinberger, Phys. Rev. B **65**, 125101 (2002).
[30] *Electron Scattering in Solid Matter*, edited by J. Zabloudil, R. Hammerling, L. Szunyogh, and P. Weinberger (Springer, Berlin, 2005).
[31] C. Uiberacker, J. Zabloudil, P. Weinberger, L. Szunyogh, and C. Sommers, Phys. Rev. Lett. **82**, 1289 (1999).
[32] J. Henk, A. M. N. Niklasson, and B. Johansson, Phys. Rev. B **59**, 9332 (1999).
[33] G. Nicolay, F. Reinert, S. Hüfner, and P. Blaha, Phys. Rev. B **65**, 033407 (2001).
[34] J. Henk, A. Ernst, and P. Bruno, Phys. Rev. B **68**, 165416 (2003).
[35] F. Reinert, J. Phys.: Condens. Matter **15**, S693 (2003).
[36] J. Henk, M. Hoesch, J. Osterwalder, A. Ernst, and P. Bruno, J. Phys.: Condens. Matter **16**, 7581 (2004).
[37] J. Henk, A. Ernst, K. K. Saha, and P. Bruno, J. Phys.: Condens. Matter **18**, 2601 (2006).
[38] P. Weinberger, *Electron Scattering Theory of Ordered and Disordered Matter* (Clarendon Press, Oxford, 1990).
[39] I. Mertig, E. Mrosan, and P. Ziesche, *Multiple Scattering Theory of Point Defects in Metals: Electronic Properties* (B. G. Teubner, Leipzig, 1987).
[40] A. Gonis, *Green Functions for Ordered and Disordered Systems*, Studies in Mathematical Physics, Vol. 4 (North-Holland, Amsterdam, 1992).
[41] J. Henk, in *Handbook of Thin Film Materials*, edited by H. S. Nalwa (Academic Press, San Diego, 2001), Vol. 2, Chap. 10, p. 479.
[42] E. M. Rose, *Relativistic Electron Theory* (Wiley & Sons, New York, 1961).
[43] P. Strange, *Relativistic Quantum Mechanics: With Applications in Condensed Matter and Atomic Physics* (Cambridge University Press, Cambridge, U.K., 1998).
[44] E. Tamura, Phys. Rev. B **45**, 3271 (1992).
[45] J. S. Faulkner and G. M. Stocks, Phys. Rev. B **21**, 3222 (1980).
[46] J. Henk and P. Bruno, Phys. Rev. B **68**, 174430 (2003).
[47] J. Mathon and A. Umerski, Phys. Rev. B **60**, 1117 (1999).
[48] J. Mathon and A. Umerski, Phys. Rev. B **63**, 220403(R) (2001).
[49] J. B. Pendry, A. B. Prête, and B. C. H. Krutzen, J. Phys.: Condens. Matter **3**, 4313 (1991).
[50] J. M. MacLaren, X.-G. Zhang, W. H. Butler, and X. Wang, Phys. Rev. B **59**, 5470 (1999).
[51] D. S. Fisher and P. A. Lee, Phys. Rev. B **23**, 6851 (1981).
[52] R. Evarestov and V. Smirnow, Phys. Status Solidi B **119**, 9 (1983).
[53] J. Henk, Phys. Rev. B **64**, 035412 (2001).
[54] K. Palotás, B. Lazarovits, L. Szunyogh, and P. Weinberger, Phys. Rev. B **70**, 134421 (2004).
[55] G. Metalidis and P. Bruno, Phys. Rev. B **72**, 235304 (2005).
[56] N. D. Lang, Phys. Rev. Lett. **56**, 1164 (1986).
[57] N. D. Lang, Phys. Rev. B **34**, 5947 (1986).
[58] N. D. Lang, Phys. Rev. B **36**, 8173 (1987).
[59] Y. Y. Sharvin, Sov. Phys. JETP **21**, 655 (1965).
[60] K. Palotás, B. Lazarovits, L. Szunyogh, and P. Weinberger, Phys. Rev. B **67**, 174404 (2003).
[61] V. Popescu, H. Ebert, N. Papanikolaou, R. Zeller, and P. H. Dederichs, J. Phys.: Condens. Matter **16**, S5579 (2004).
[62] P. Mavropoulos, N. Papanikolaou, and P. H. Dederichs, Phys. Rev. B **69**, 125104 (2004).
[63] C. Tusche, H. L. Meyerheim, N. Jedrecy, G. Renaud, A. Ernst, J. Henk, P. Bruno, and J. Kirschner, Phys. Rev. Lett. **95**, 176101 (2005).
[64] A. Gonis, A. J. Freeman, and P. Weinberger, Phys. Rev. B **32**, 7713 (1985).
[65] N. Stefanou, P. J. Braspenning, R. Zeller, and P. H. Dederichs, Phys. Rev. B **36**, 6372 (1987).
[66] L. Olesen, M. Brandbyge, M. R. Sørensen, K. W. Jacobsen, E. Lægsgaard, I. Stensgaard, and F. Besenbacher, Phys. Rev. Lett. **76**, 1485 (1996).
[67] R. Z. Huang, V. S. Stepanyuk, A. L. Klavsyuk, W. Hergert, P. Bruno, and J. Kirschner, Phys. Rev. B **73**, 153404 (2006).
[68] M. Brandbyge, J.-L. Mozos, P. Ordejon, J. Taylor, and K. Stokbro, Phys. Rev. B **65**, 165401 (2002).
[69] H. F. Ding, W. Wulfhekel, J. Henk, P. Bruno, and J. Kirschner, Phys. Rev. Lett. **90**, 116603 (2003).
[70] N. D. Lang, Phys. Rev. B **37**, 10395 (1988).
[71] J. M. Pitarke, P. M. Echenique, and F. Flores, Surf. Sci. **217**, 267 (1989).
[72] K. Palotás and W. A. Hofer, J. Phys.: Condens. Matter **17**, 2705 (2005).
[73] W. A. Hofer and A. Garcia-Lekue, Phys. Rev. B **71**, 085401 (2005).
[74] M. Woods, A. Ernst, P. Strange, and W. M. Temmerman, J. Phys.: Condens. Matter **13**, 8607 (2001).
[75] M. Lüders, A. Ernst, W. M. Temmerman, Z. Szotek, and P. J. Durham, J. Phys.: Condens. Matter **13**, 8587 (2001).
[76] A. Ernst, J. Henk, and R. K. Thapa, J. Phys.: Condens. Matter **17**,

3269 (2005).
[77] M. Lüders, A. Ernst, M. Däne, Z. Szotek, A. Svane, D. Ködderitzsch, W. Hergert, B. L. Györffy, and W. M. Temmerman, Phys. Rev. B **71**, 205109 (2005).
[78] X.-G. Zhang and D. M. C. Nicholson, Phys. Rev. B **60**, 4551 (1999).
[79] D. M. Heyes and F. van Swol, J. Chem. Phys. **75**, 5051 (1981).
[80] J. M. Blanco, F. Flores, and R. Pérez, Prog. Surf. Sci. **81**, 403 (2006).
[81] C. R. Ast, J. Henk, A. Ernst, L. Moreschini, M. C. Falub, D. Pacilé, P. Bruno, K. Kern, and M. Grioni, Phys. Rev. Lett. **98**, 186807 (2007).
[82] A. L. Vázquez de Parga, O. S. Hernán, R. Miranda, A. Levy Yeyati, N. Mingo, A. Martin-Rodero, and F. Flores, Phys. Rev. Lett. **80**, 357 (1998).
[83] F. Reinert and G. Nicolay, Appl. Phys. A: Mater. Sci. Process. **78**, 817 (2004).
[84] S. LaShell, B. A. McDougall, and E. Jensen, Phys. Rev. Lett. **77**, 3419 (1996).
[85] R. Z. Huang, V. S. Stepanyuk, and J. Kirschner, J. Phys.: Condens. Matter **18**, L217 (2006).
[86] D. Wortmann, H. Ishida, and S. Blügel, Phys. Rev. B **72**, 235113 (2005).
[87] P. M. Levy, K. Wang, P. H. Dederichs, C. Heide, S. Zhang, and L. Szunyogh, Philos. Mag. B **82**, 763 (2002).
[88] H. Ishida, D. Wortmann, and T. Ohwaki, Phys. Rev. B **70**, 085409 (2004).
[89] R. M. Tromp, E. J. van Loenen, J. E. Demuth, and N. D. Lang, Phys. Rev. B **37**, 9042 (1988).
[90] E. Merzbacher, *Quantum Mechanics*, 2nd ed. (John Wiley & Sons, New York, 1970).
[91] J. C. Slonczewski, Phys. Rev. B **39**, 6995 (1989).
[92] J. Staunton, B. L. Gyorffy, A. J. Pindor, G. M. Stocks, and H. Winter, J. Magn. Magn. Mater. **45**, 15 (1984).